HAL
open science

15 Deoxi-Δ-Prostaglandin j is a tubulin-binding agent that destabilizes microtubules and induces mitotic arrest

Claudia Cocca, Jorge Dorado, Enrique Calvo, Juan Antonio López, Angel Santos, Ana Perez-Castillo

To cite this version:

Claudia Cocca, Jorge Dorado, Enrique Calvo, Juan Antonio López, Angel Santos, et al.. 15 Deoxi-Δ-Prostaglandin j is a tubulin-binding agent that destabilizes microtubules and induces mitotic arrest. Biochemical Pharmacology, 2009, 78 (10), pp.1330. 10.1016/j.bcp.2009.06.100 . hal-00522544

HAL Id: hal-00522544

https://hal.science/hal-00522544v1

Submitted on 1 Oct 2010

HAL is a multi-disciplinary open access archive for the deposit and dissemination of scientific research documents, whether they are published or not. The documents may come from teaching and research institutions in France or abroad, or from public or private research centers.

L'archive ouverte pluridisciplinaire **HAL**, est destinée au dépôt et à la diffusion de documents scientifiques de niveau recherche, publiés ou non, émanant des établissements d'enseignement et de recherche français ou étrangers, des laboratoires publics ou privés.

Accepted Manuscript

Title: 15 Deoxi-$\Delta^{12,14}$-Prostaglandin j_2 is a tubulin-binding agent that destabilizes microtubules and induces mitotic arrest

Authors: Claudia Cocca, Jorge Dorado, Enrique Calvo, Juan Antonio López, Angel Santos, Ana Perez-Castillo

PII: S0006-2952(09)00592-9
DOI: doi:10.1016/j.bcp.2009.06.100
Reference: BCP 10248

To appear in: *BCP*

Received date: 29-4-2009
Revised date: 18-6-2009
Accepted date: 24-6-2009

Please cite this article as: Cocca C, Dorado J, Calvo E, López JA, Santos A, Perez-Castillo A, 15 Deoxi-$\Delta^{12,14}$-Prostaglandin j_2 is a tubulin-binding agent that destabilizes microtubules and induces mitotic arrest, *Biochemical Pharmacology* (2008), doi:10.1016/j.bcp.2009.06.100

This is a PDF file of an unedited manuscript that has been accepted for publication. As a service to our customers we are providing this early version of the manuscript. The manuscript will undergo copyediting, typesetting, and review of the resulting proof before it is published in its final form. Please note that during the production process errors may be discovered which could affect the content, and all legal disclaimers that apply to the journal pertain.

* Manuscript
ACCEPTED MANUSCRIPT

15 DEOXI-$\Delta^{12,14}$-PROSTAGLANDIN J_2 IS A TUBULIN-BINDING AGENT THAT DESTABILIZES MICROTUBULES AND INDUCES MITOTIC ARREST.

Claudia Cocca[1,2*], Jorge Dorado[1*], Enrique Calvo[3], Juan Antonio López[3], Angel Santos[4], and Ana Perez-Castillo[1].

Abbreviated title: Mitotic arrest induced by 15d-PGJ_2.

[1]Instituto de Investigaciones Biomédicas, Consejo Superior de Investigaciones Científicas-Universidad Autónoma de Madrid and Centro de Investigación Biomédica en Red sobre Enfermedades neurodegenerativas (CIBERNED, 28029-Madrid, Spain.
[2]Present address: Laboratorio de Radioisótopos. Facultad de Farmacia y Bioquímica. Universidad de Buenos Aires. C1113ABB-Bs.As, Argentina.
[3]Unidad de Proteómica. Centro Nacional de Investigaciones Cardiovasculares, Melchor Fernández Almagro, 3, 29029-Madrid, Spain
[4]Departamento de Bioquímica y Biología Molecular. Facultad de Medicina, Universidad Complutense de Madrid, 28040-Madrid, Spain.

*Both authors contributed equally to this work

Address correspondence to: Ana Perez-Castillo. Instituto de Investigaciones Biomédicas, Consejo Superior de Investigaciones Científicas-Universidad Autónoma de Madrid. Arturo Duperier, 4. 28029-Madrid. Spain. Phone: 34-91-5854436, Fax: 34-91-5854401, e-mail: aperez@iib.uam.es or to: Angel Santos. Departamento de Bioquímica y Biología Molecular, Facultad de Medicina, Universidad Complutense, Madrid. Spain. Phone: 34-91-3941446. Fax: 34-91-3941691, e-mail: piedras3@med.ucm.es

Accepted Manuscript

ACCEPTED MANUSCRIPT

ABSTRACT:

15-deoxi-$\Delta^{12,14}$-prostaglandin J_2 (15d-PGJ_2) is known to play an important role in the pathophysiology of carcinogenesis, however the molecular mechanisms underlying these effects are not yet fully understood. Recently, we have shown that 15d-PGJ_2 is a potent inducer of breast cancer cell death and that this effect is associated with a disruption of the microtubule cytoskeletal network. Here, we show that treatment of the MCF-7 breast cancer cell line with 15d-PGJ_2 induces an accumulation of cells in the G_2/M compartment of the cell cycle and a marked disruption of the microtubule network. 15d-PGJ_2 treatment causes mitotic abnormalities that consist of failure to form a stable metaphase plate, incapacity to progress through anaphase, and failure to complete cytokinesis. 15d-PGJ_2 binds to tubulin through the formation of a covalent adduct with at least four cysteine residues in α- and β-tubulin, as detected by hybrid triple-quadrupole mass spectrometry analysis. Overall, these results support the hypothesis that microtubule disruption and mitotic arrest, as a consequence of the binding of 15d-PGJ_2 to tubulin, can represent one important pathway leading to breast cancer cell death.

Keywords: 15d-PGJ_2, cell death, cytoskeleton, mitosis, tubulin, cancer.

Accepted Manuscript

ACCEPTED MANUSCRIPT

INTRODUCTION

Cyclopentenone prostaglandins are potent bioactive molecules involved in regulating many physiological as well as pathological processes [1, 2]. Some of these prostaglandins have been shown to induce cell cycle arrest and apoptosis in a number of cancer cell types [3]. In particular, the terminal derivative of prostaglandin J_2 metabolism, 15-deoxi-$\Delta^{12,14}$-prostaglandin J_2 (15d-PGJ_2), is emerging as the most potent antineoplastic agent of this class of prostaglandins. Anticancer activity of 15d-PGJ_2 has been reported both in vitro and in vivo in a multiplicity of tissues including breast, prostate, colon, lung, brain, skin, and lymphoid [4-11]. However, the mechanism of 15d-PGJ_2 antineoplastic activity has not been fully elucidated as yet.

Although 15d-PGJ_2 was identified as a high-affinity natural ligand for peroxisome proliferators-activated receptor (PPAR) γ [12], it is now thought to exert its effects through PPARγ-dependent and –independent mechanisms. Among these PPARγ-independent mechanisms are pathways that operate through NF-κB and AP1, and other signal transducers and activators of transcription [13-16]. 15d-PGJ_2 has also been reported to induce apoptosis of several types of cancer cells and normal cells independently of PPARγ activation including breast cancer cells, dentritic cells, and hepatic myofibroblasts [17-19]. For example, hepatic myofibroblasts do not express PPARγ, but still undergo apoptosis when exposed to 15d-PGJ_2. We have also reported that 15d-PGJ_2 is a potent inhibitor of mitochondrial function through PPARγ-independent means [20].

We have recently shown that 15d-PGJ_2 inhibits neoplastic breast cancer cell proliferation, induces apoptosis, and disrupts microtubule (MT) assembly, suggesting

ACCEPTED MANUSCRIPT

that the anti-neoplastic effects of 15d-PGJ_2 can be triggered by multiple mechanisms, one of them probably involving MT dynamics [8]. Microtubules are the principal components of the cytoskeleton network of eukaryotic cells and have been shown to be involved in various cellular functions, including cell division, cytokinesis, maintenance of cell morphology, and signal transduction [21, 22] Microtubules are intracellular, filamentous, polymeric structures composed of two structurally similar protein subunits, namely, α- and β-tubulin (molecular weight, 50 kDa each). During mitosis, microtubules undergo rapid polymerization and depolymerization to enable movement of chromosomes. As cell division approaches metaphase, microtubules are disrupted and form a spindle surrounding the centrosome, thereby facilitating chromosomal alignment on the metaphase plate. In this process, tubulin subunits freely exchange on the microtubules. If such free exchange of tubulin subunits is disrupted, the mitotic spindle is compromised and the cell cannot divide. Certain drugs have already been discovered which bind tubulin (e.g., Vinca alkaloids and the colchicine-site binders), thereby preventing them from being incorporated into growing microtubules. As a consequence cells undergoing division, and particularly those cells showing rapid division (i.e., cancer cells), are killed. Thus, in the field of antineoplastic chemotherapy, anti-microtubule agents constitute an important class of compounds, with broad activity both in solid tumors and in hematological malignancies [21, 23, 24].

Here, we show that upon treatment with 15d-PGJ_2, MCF-7 breast cancer cell line arrest at the G_2/M phase of the cell cycle. 15d-PGJ_2 also causes a depolymerization of the microtubule network and inhibits assembly of purified tubulin in vitro, probably due to the covalent modification of at least four cysteine residues in polymerized α- and β-tubulin. This microtubule disorganization is accompanied by mitotic abnormalities and

ACCEPTED MANUSCRIPT

incapacity to progress through anaphase. This study identifies tubulin as a molecular target of the pro-apoptotic 15d-PGJ_2 compound.

Accepted Manuscript

ACCEPTED MANUSCRIPT

MATERIALS AND METHODS

Cell culture. MCF-7 human mammary epithelial cells were grown as previously described [7]. For microscopy experiments cells were grown on glass coverslips. Experimental cultures were stimulated with the appropriate ligand, as indicated.

Antibodies. Pericentrin rabbit polyclonal antibody was from Covance (Berkeley, California). Mouse monoclonal anti-α-tubulin (Clone DM 1A) and anti-β-tubulin (Clone SDL.3D10) antibodies were from Sigma (St Louis, MO). Biotin goat polyclonal and Alexa secondary antibodies were from Vector Laboratories (Burlingame, USA)

*Cell cycle analysis***.** MCF-7 cells were treated with 10 μM 15dPG-J_2 (Cayman Chemical, MI, USA) or 30 μM rosiglitazone (Cayman Chemical, MI, USA) in regular RPMI medium for 24 h. Cells were then fixed in 70% ethanol/PBS, pelleted and resuspended in buffer containing 10 μg/ml RNAse A and 0.01 mg/ml propidium iodide. Cell cycle distribution was determined by flow cytometric analysis utilizing a Cyan MLE-R Cytometer (DAKO-Cytomation, Glastrup, Denmark). Data analysis was performed using the Summit Software (DAKO).

In vitro tubulin polymerization assay**.** In vitro tubulin assembly was evaluated using the HTS-Tubulin Polimerization Assay Kit (Cytoskeleton, Denver, CO), according to the manufacturer's instructions. Absorbance readings were taken at 340 nm every 30 s for 1 h, using a Varioscan (Thermo Electron Corporation) plate reader and Skanit 2.0 Research Edition.

ACCEPTED MANUSCRIPT

*Separation of soluble and polymerized tubulins***.** Separation of soluble and polymerized tubulins was carried out as described by Minotti et al [25]. Briefly, 12 h after 15d-PGJ_2 (10 μM) or rosiglitazone (30 μM) treatment, MCF-7 cells were lysed using 120 μl of microtubule-stabilizing buffer [20 nM Tris-HCl (pH 6.8), 1 mM $MgCl_2$, 2 mM EGTA, 0.5% NP-40, 2 mM PMSF, 1 mM benzamidine]. After vortexing, 120 μg of protein were centrifuged at 13,000 rpm for 15 minutes at room temperature and soluble (supernatant) and polymerized (pellet) tubulin analyzed by SDS-PAGE and immunoassay as described [8].

*Biotinylated 15dPG-J_2 pull down and western blot analysis***.** For in vivo incorporation of 15d-PGJ_2 into α- and β-tubulin in intact cells, MCF-7 cells were incubated with 10 μM biotinylated 15d-PGJ_2 for 2 h, lysed in lysis buffer [10 mM Tris-HCl (pH 7.5), 0.1 mM EDTA, 0.1 mM EGTA, 0.5% SDS, 0.1 mM 2-mercaptoethanol and 1mM PMSF], and biotinylated proteins were purified by adsorption onto Neutravidin beads (Pierce Biotechnology, Inc. Rockford, IL), as described by the manufacturer's. Proteins were detected by Western blot using anti-α- and anti-β antibodies, as previously described [8].

Immunofluorescence and confocal microscopy. Confocal microscopy was used to detect cytoskeleton organization. MCF-7 cells were plated on glass coverslips in 24-well cell culture plates and grown in regular medium for 12 h before switching to new medium with the corresponding treatment. Cells were then fixed for 10 min with methanol at –20°C, and washed with PBS. After one hour incubation with the appropriate primary antibody, cells were washed and incubated with DAPI, Alexa Fluor 488, Alexa Fluor 546, or Alexa Fluor 647 secondary antibodies (Molecular Probes) for 45 min at 37°C.

ACCEPTED MANUSCRIPT

Images were acquired using a Radiance 2100 laser scanning confocal microscope (Bio-Rad, Hercules, CA) using a 60x NA 1.40 oil immersion objective (Nikon). The images were obtained using a series of 0.5 μm (depth) spaced cell fluorescent slices (Z axis). Confocal microscope settings were adjusted to produce the optimum signal-to-noise ratio. Images were collected and processed using Lasersharp 2000 and Adobe Photoshop version 8.0, respectively.

*Time-Lapse microscopy***.** MCF-7 cells were plated and placed in a chamber in complete medium with CO_2 exchange at 37ºC. Cells were imaged every 1 min for 1-2 days using a 40x objective on an inverted microscope (Zeiss Axiovert 135 TV). Images were captured on a JVC (TK-C1481EG) digital video camera. Where indicated, 10 μM 15d-PGJ_2 or 30 μM rosiglitazone were added to live microscopy media. Resulting movies were collected and processed by using image analySIS software (Soft Imaging System) and exported as Quicktime (Apple Computer, Cupertino, CA) and are shown at 7 frames per second (Supplemental videos 1-3 online).

Off line nanospray characterization of 15d-PGJ_2 by mass spectrometry. About 1 μl containing 5 μg of 15d-PGJ_2 was dissolved in 20 μl of 50% CH3CN, 0.5% acetic acid. 5 μl was introduced into the off line nanospray medium needle and infused using the Protana nanosprayTM ion source. The 15d-PGJ_2 was ionized into a triple quadrupole mass spectrometer (4000 Q Trap LC-MS/MS hybrid system, Applied Biosystems, MDS Sciex), and data were acquired for 2 min. The needle voltage was set at 1300 V, and the declustering potential was set at 50 V to minimize in-source fragmentation. A collision energy between 25 and 30 was used to induce the fragmentation of the 15d-PGJ_2 molecule.

ACCEPTED MANUSCRIPT

Protein digestion and sample preparation for MS analysis. Untreated or 15d-PGJ_2-treated microtubules samples were incubated with 1 µg trypsin (Promega Sequencing Grade) for 2 h at 37ºC. Reaction mixtures were dried in vacuo and dissolved in 5% CH3CN, 0.5% CH3COOH, for later MS analysis.

Nano-HPLC and tandem triple-quadrupole MS analysis of peptides. The tryptic peptides from control, and 15d-PGJ_2-treated samples were injected with a Famos (LC Packings) autosampler onto a PepMapTM C18 reversed phase micro-column (300 µm ID x 5 mm) from LC Packings and washed to remove salts. Samples were eluted onto a C18 reversed phase nano-column (100 µm ID x 15 cm, Teknokroma, Mediterranea sea), which was developed with a CH3CN gradient (5-47.5% CH3CN over 45 min, followed by a 1 min increase to 85.5% CH3CN) generated by an Ultimate Nano-HPLC (LC Packings). A flow rate of ca. 300 nl min-1 was used to elute peptides from the nano-column to a New Objective PicoTip™ emitter nano-spray needle (3000 V) in a Protana nanospray ion source, and ions were analyzed with the 4000 Q-Trap system. In the enhanced resolution mode, the linear ion trap was scanned at m/z 250/s, and the ion of interest was selected in Q1 by precursor ion scanning. N2 was used as the curtain (value of 15) and collision gas (set to high).

Multiple Reaction Monitoring (MRM). 15d-PGJ_2-bound tryptic peptides from treated and untreated microtubules were analyzed in the MRM mode. Q1 was set on the m/z corresponding to charged parent ions from masses 1, 2, 3, and 4 previously observed (see results; m/z at 644.4, 662.9, 726.4, and 989.9, respectively), and Q3 was set on specific fragment ions for each parent mass (m/z at 482.3 corresponding to y4 fragment

ACCEPTED MANUSCRIPT

ion for mass 1, m/z at 948.2 corresponding to 15d-PGJ_2-modified y6 fragment ion for mass 2, m/z at 841.4 corresponding to y7 fragment ion for mass 3, and m/z 1326.1 corresponding to doubly-charged, y25 fragment ion for mass 4; Supplementary Fig. 2). Collision energy was set to 30 eV.

MS data analysis. All the chromatograms and MS/MS spectra from the 4000 Q Trap System were analyzed with Analyst 1.4.1 software (Applied Biosystems). Analyses of 15d-PGJ_2-binding to microtubules by MS were repeated with two independent samples.

Statistical analysis. The data shown are the means±s.d. of at least three independent experiments. Statistical comparisons for significance between cells with different treatments were performed using the Student's t test.

Accepted Manuscript

ACCEPTED MANUSCRIPT

RESULTS

15d-PGJ$_2$ arrests the cell cycle at G$_2$/M phase and causes a disruption of MCF-7 microtubule network. To determine the effect of 15d-PGJ$_2$ on cell cycle, exponentially growing MCF-7 cells were treated with 15d-PGJ$_2$ for 24 h and their cell cycle progression was followed by fluorescence activated cell sorting analysis. Fig. 1 demonstrates that treatment with 15d-PGJ$_2$ led to significant increased numbers of G$_2$/M phase cells, compared with non-treated control cells. On the contrary, the percentage of cells in the G$_2$/M cell cycle state did not differ markedly between control and MCF-7 cells treated with rosiglitazone (RSG), a specific synthetic PPARγ agonist. Nocodazole, a potent anti-microtubule agent capable of rapidly depolymerizing the MT network, was used as control [26].

It has been very well documented that MT inhibitors are known to arrest cells in G$_2$/M phase and induce cell death [21, 22]. Based on this observation, and our previous results [8], we then reasoned that the induction of G$_2$/M arrest by 15d-PGJ$_2$ could be attributed to the disruption of the cytoskeleton. To test this hypothesis, we first examined whether 15d-PGJ$_2$ could directly affect the organization of the MT network of MCF-7 cells in the interphase phase. To this end, MCF-7 cells were treated with 15d-PGJ$_2$, rosiglitazone, or nocodazole and the MT network was visualized by immunofluorescence after 12 h of incubation. In control cells, the MT network exhibited normal arrangement with MT seen to traverse intricately throughout the cell and a normal compact rounded nucleus (Fig. 2A). In contrast, 15d-PGJ$_2$ treatment led to a dramatic disruption of the MCF-7 cytoskeleton, producing a diffuse MT network. These effects, which are similar to those exerted by nocodazole, were not observed after

ACCEPTED MANUSCRIPT

rosiglitazone treatment. The multiple-dot pericentrin pattern obtained is characteristic of certain breast cancer cell lines [27] and was corroborated by γ-tubulin staining (data not shown).

To further demonstrate that 15d-PGJ_2 could promote MT depolymerization *in vivo*, we next investigated the fraction of free and polymerized α-tubulin in control and 15d-PGJ_2-treated MCF-7 cells, specifically by harvesting the cells in a MT-stabilizing buffer and performing differential sedimentation. Our results indicate that the amount of polymerized α-tubulin in the pellet fraction was significantly decreased 12 h after treatment of MCF-7 cells with 15d-PGJ_2, when compared with basal cultures (Fig 2B, C). In contrast, we could not observe any decrease in polymerized tubulin after treatment with rosiglitazone, in comparison with control non-treated MCF-7 cells.

Mitotic abnormalities following 15d-PGJ_2 treatment. Microtubule targeting agents are known to arrest the cell cycle in early mitosis i.e. prometaphase/metaphase. Therefore, we next investigated the effect of 15d-PGJ_2 on MCF-7 cell division. We first examined mitotic figures in MCF-7 cells treated or not with 15d-PGJ_2 for 24 h, fixed and co-stained with DAPI and anti-α-tubulin and anti-pericentrin antibodies to monitor DNA, the mitotic spindle, and the centrosomes, respectively. Cell morphology and the percentage of cells at different stages of mitosis and cytokinesis were determined using a confocal microscope. Control cells with no added 15d-PGJ_2 rounded up at the beginning of mitosis and split into two symmetrical daughter cells as expected (Fig. 3A). In contrast, although 15d-PGJ_2-treated cells developed spindle-like structures (Fig. 3B), the MT fibers generally lack the organization observed in control cells. Also, in the cultures treated with 15d-PGJ_2, we could not detect any cell proceeding to either

ACCEPTED MANUSCRIPT

anaphase or telophase/cytokinesis and these cells displayed distinct signs of arrest in the metaphase stage of mitosis as the nuclear membrane has disappeared and the chromatin was condensed. The major changes, however, were the complete absence of anaphase and telophase cells and the large increase in the percentage of metaphase cells exhibiting metaphase plates with incomplete chromosome alignment, following 15d-PGJ_2 treatment. Cells with such characteristics were unable to undergo cytokinesis. The stage of mitosis at which the block occurred was further determined by counting the number of cells at each stage of mitosis. As shown in Fig. 3C, in the 15d-PGJ_2-treated MCF-7 cells, the number of cells in anaphase and telophase/cytokinesis decreased to zero, indicating a block specifically at the transition from metaphase to anaphase. These results suggest that 15d-PGJ_2 acts as a mitotic inhibitor.

Time-lapse microscopy was utilized to characterize the fate of MCF-7 cells treated with 15d-PGJ_2 and rosiglitazone (Fig. 4 and Supplementary Videos 1-3 online). We have found that the majority of control non-treated cells undergo cell division within 80 to 90 min (Fig. 4 and Supplementary Video 1 online). Non-treated cells were able to segregate chromosomes, proceed through anaphase, initiate furrow formation and elongate the midbodies. Eventually the cells segregate and flatten out. However, the majority of 15d-PGJ_2-treated cells took 3 h or longer for a significant number of cells to proceed to metaphase. During that time, cells could go through the nuclear envelope breakdown but they were unable to form a stable metaphase plate with all the chromosomes aligned to it and eventually proceed to anaphase. The single prominent phenotype associated with 15d-PGJ_2 treatment was failure to complete cytokinesis. After more than 7 h in a “metaphase-like” stage, cells eventually shriveled and died (Fig. 4 and Supplementary Video 2 online). When MCF-7 cells were treated with

ACCEPTED MANUSCRIPT

rosiglitazone, no significant differences in the process of mitosis were observed (Fig. 4 and Supplementary Video 3 online). Cells treated with rosiglitazone were able to complete mitosis within a period of time similar to the one observed for control non-treated cells. When taken together with the images shown in Fig. 3, these results provide compelling evidence that treatment of MCF-7 cells with 15d-PGJ_2 results in failure of cell division through arrested metaphase.

Effect of 15d-PGJ_2 on tubulin polymerization in vitro. Because 15d-PGJ_2 markedly disrupted the cellular MT network, we tested whether 15d-PGJ_2 could directly affect tubulin, the main component of this network. An in vitro biochemical tubulin polymerization assay was carried out to investigate the activity of 15d-PGJ_2 on MT function. Results presented in Fig. 5 shows that 15d-PGJ_2 significantly inhibited the polymerization of tubulin, similar to the effect elicited by nocodazole, a well-known MT destabilizer. On the contrary, the addition of paclitaxel, in agreement with previous reports, favors tubulin polymerization. In contrast, rosiglitazone was found to have a negligible effect upon the polymerization of tubulin in vitro, relative to the vehicle control (data not shown), in agreement with its lack of effect upon the cellular MT network. This again, distinguishes the mechanism of action of both PPARγ ligands and suggests that the effects of 15d-PGJ_2 are independent of PPARγ activation. These data suggest that 15d-PGJ_2 could bind directly to tubulin and thereby prevent its polymerization and identify tubulin as a molecular target of 15d-PGJ_2.

The possibility that 15d-PGJ_2 could directly bind to, both α- and β-tubulin in vivo was investigated by using a biotinylated 15d-PGJ_2 derivative. To this end, we first analyzed the incorporation of biotinylated 15d-PGJ_2 into α- and β-tubulin by

ACCEPTED MANUSCRIPT

Neutravidin-gel pull down followed by Western blot with anti-α-tubulin or anti-β-tubulin antibodies. Fig. 6A shows that α- and β-tubulin present in lysates from biotinylated 15d-PGJ_2-treated MCF-7 cells were retained on Neutravidin beads, suggesting that 15d-PGJ_2 is able to react with endogenous α- and β-tubulin in intact MCF-7 cells. To further analyze the *in vivo* association between tubulin and 15d-PGJ_2 in the living cell, we performed confocal microscopy analysis of MCF-7 cells treated or not with biotinylated 15d-PGJ_2 for 2 h and stained with anti-α- or anti-β-tubulin. As shown in Fig. 6B, a biotinylated 15d-PGJ_2 network, which colocalized with the endogenous tubulin network was clearly seen. This colocalization is also observed as the cell progresses into the cell cycle (Fig. 6C). These results further suggest a direct binding between 15d-PGJ_2 and the MT network.

Binding of 15d-PGJ_2 to tubulin. The above results indicate that 15d-PGJ_2 binds to both α- and β-tubulin, therefore we next analyzed untreated and 15d-PGJ_2-treated microtubules samples by mass spectrometry (MS) to characterize the binding site(s) of 15d-PGJ_2 within the tubulin. We used a recently reported approach based on hybrid triple-quadrupole mass spectrometry to find the 15d-PGJ_2-binding site(s) [28].

We first made the characterization of 15d-PGJ_2 molecule by off line mass spectrometric analysis, and an ion at m/z 317.4 Da, corresponding to the monoisotopic, protonated 15d-PGJ_2 molecule, was observed (Supplementary Fig. 1A). In order to find the main fragments corresponding to single or multiple cleavage sites within the 15d-PGJ_2 molecule, an enhanced product ion experiment was performed (Supplementary Fig. 1B). The most intense fragment ions were selected as potential markers for later precursor ion scanning experiments. The fragment ion at m/z 299.4 Da, out of the seven

ACCEPTED MANUSCRIPT

tested (145.2, 169.2, 183.2, 197.2, 215.4, 281.4, and 299.4), was the signal of choice for precursor ion filtering experiments (Supplementary Fig. 1C). The efficiency of precursor ion scanning experiments was lower when using the other seven fragment ions present in the MS/MS spectrum from the 15d-PGJ_2 molecule (Supplementary Fig 1C).

Precursor ion scanning-MS chromatograms of trypsin-digested microtulules from untreated (Fig. 7A, upper panel) or 15d-PGJ_2-treated (Fig. 7A, lower panel) samples were analyzed. Although no differential, intense chromatographic peaks were found, an exhaustive mass composition chromatographic analysis revealed six time positions (1-6 in Fig. 7A) along the chromatograms corresponding to differential signals producing the 15d-PGJ_2-derived fragment ion at m/z 299.4 Da. These time positions marked the elution time for differential signals tagged with 15d-PGJ_2 (Fig. 7B), which were only present in the 15d-PGJ_2-treated sample, as indicated by the asterisks (Fig. 7B).

MS/MS-based peptide sequencing of differential masses 1, 2, and 4 (Supplementary Figs. 2A, 2B, and 2D, respectively) demonstrated that these sequences (353-TAVC^{PG}DIPPR-361, 300-NMMAAC^{PG}DPR-308, and 219-LTTPTYGDLNHLVSATMSGVTTC^{PG}LR-243, respectively) mapped into β-tululin, while the sequences from differential masses 3 (312-YMACC^{PG}LLYR-320), and 5 (309-HGKYMACC^{PG}LLYR-320; one missed cleavage at K311; not shown) corresponded to α-tubulin-derived peptides (Supplementary Fig. 2C). A comprehensive study of the fragmentation spectra from the parent ions corresponding to masses 1-5 revealed that in all cases the cysteine within the sequence was the 15d-PGJ_2-binding residue (superscripted PG-cysteine in text and Supplementary Fig. 2). For peptides 3

ACCEPTED MANUSCRIPT

and 5, only one of the two cysteine residues was modified by 15d-PGJ_2. Differential mass 6 corresponded to the unbound 15d-PGJ_2 dimer, appearing later on the chromatogram due to the highly hydrophobic nature of the molecule.

These results were verified by Multiple Reaction Monitoring (MRM) experiments (Fig. 8). Ions at m/z 644.4, 662.9, 726.4, and 989.9 (corresponding to differential masses 1, 2, 3, and 4, respectively) were isolated and fragmented in untreated and 15d-PGJ_2-treated microtubules samples. As can be observed, only in the 15d-PGJ_2-treated chromatogram, the four differential, intense chromatographic peaks were detected (Fig. 8).

Accepted Manuscript

ACCEPTED MANUSCRIPT

DISCUSSION

Although it has been clearly established that 15d-PGJ_2 is a potent inducer of cell death in many cancer cell lines, including human breast cancer cells, our knowledge of the mechanisms of action by which 15d-PGJ_2 causes cell death remains incomplete. In the present study, we show that cell death induced by 15d-PGJ_2 in human MCF-7 cells is preceded by a marked G_2/M arrest. The cells also displayed morphological features that identified a mitotic arrest, specifically in metaphase. Our studies also show that 15d-PGJ_2 binds to microtubules, forming a covalent bond with several cysteine residues in α- and β-tubulin. Overall these results point to a role of 15d-PGJ_2 in breast cancer cells independent of PPARγ activation and possibly involving a direct binding to tubulin and posterior disruption of microtubules. This idea is further substantiated by the fact that these effects are not observed in rosiglitazone-treated MCF-7 cells.

We have previously demonstrated that 15d-PGJ_2 inhibits proliferation and induces cellular differentiation and apoptosis in the breast cancer cell line MCF-7, in part by blocking the ErbB receptor signaling pathway [7] and by inducing early mitochondrial alterations [8]. Our results suggest that the effects of 15d-PGJ_2 can be, both dependent and independent of PPARγ activation [8, 20, 29]. This is in accordance with the description by other groups of PPARγ-independent pleiotropic effects of 15d-PGJ_2 responsible for its antiproliferative activity [30, 31]. Our data also indicated a possible involvement of the cytoskeleton in this process [8]. Consistent with this idea, in this study we demonstrate that 15d-PGJ_2 treatment of MCF-7 cells causes extensive MT depolymerization and disruption of the MT network in interphase cells, similar to the one observed in cells treated with nocodazole. This effect is probably due to the observed in vitro and in vivo binding of 15d-PGJ_2 to, both α– and β-tubulin subunits.

ACCEPTED MANUSCRIPT

Centrosomes abnormalities are hallmarks of various cancers and are found in essentially all high-grade cancers and in cell lines derived from tumors [32-37]. These anomalies are usually associated with an increase in pericentrin staining and the appearance of clusters of pericentrin staining material, which may represent multiple centrosomes clumped together at a single pole or an inappropriate accumulation of pericentrin. On the contrary, non-tumor tissues present a low level of diffuse staining, probably reflecting the modest level of cytoplasmic pericentrin known to be present in normal cells, or a single discrete focus of pericentrin [35]. Our results show that, in the presence of 15d-PGJ_2, MCF-7 cells exhibited fewer pericentrin foci and pericentrin staining was considerable lower than in non-treated cells. Also, the abnormal large aggregates of pericentrin seen in control MCF-7 cells, were not observed in 15d-PGJ_2-treated cells, indicative of a less transformed phenotype.

The ability of 15d-PGJ_2 to block MCF-7 cells in G_2/M phase is consistent with a disruption of cytoskeleton via binding to tubulin [38]. Among novel drugs for the treatment of advanced breast cancer are those that target microtubules. These drugs suppress microtubule dynamics and trigger mitotic arrest at the metaphase/anaphase transition [39, 40]. In the presence of these drugs, spindle form and mitosis can progress as far as the metaphase/anaphase transition. However, the spindles are completely unable to pass the mitotic cell cycle checkpoint and to initiate anaphase movements, or do so only after a long period of mitotic arrest. In agreement with this, our results show that 15d-PGJ_2 completely blocks the transition to anaphase. Only a few cells appear to enter the anaphase state but they are unable to complete the segregation of the chromosomes and eventually return to a “metaphase-like” stage afterward they die.

ACCEPTED MANUSCRIPT

There is compelling evidence that tubulin-binding agents such as paclitaxel and the vinca alkaloids kill cancer cells primarily by apoptosis [39, 41]. Because mitotic arrest caused by such agents was frequently found to precede apoptosis, a hypothesis that arrest of the cell cycle at mitosis is the primary stimulus for apoptosis has been widely accepted. For example, apoptosis induced by paclitaxel was found to occur directly after a mitotic arrest or after an aberrant mitotic exit [42, 43]. Nevertheless, some investigators have provided evidence against the involvement of mitotic arrest in apoptosis induction by microtubule-binding agents by demonstrating apoptotic events in other phases of the cell cycle [44, 45]. Apoptosis is not the only mechanism by which cells die following a failed mitosis. Many studies have described a form of cell death called mitotic catastrophe. This form of cell death does not require caspase 9 or 3 and can still occur in the presence of caspase inhibitors such as z-VAD-fmk. In this regard, previous work from our laboratory have shown that the cell death induced by 15d-PGJ_2 in breast cancer cells cannot be completely inhibited by treatment with this caspase inhibitor, albeit caspases are activated in MCF-7 cells treated with this prostaglandin [8]. On the other hand, we could not observe any of the common features attributed to mitotic catastrophe, such as giant non-viable multinucleated cells. 15d-PGJ_2-arrested mitotic MCF-7 cells appear to remain arrested in metaphase from which they subsequently entered a cell death pathway without exiting mitosis. This phenomenon has been previously shown in endothelial cells treated with the tubulin-binding agent combretastin A-4-phosphate [46, 47]. These authors have shown that combretastin A-4-phosphate damages mitotic spindles, arrests cells at metaphase, and leads to the death of endothelial mitotic cells with characteristic G_2/M DNA content.

ACCEPTED MANUSCRIPT

MS analyses also demonstrated that 15d-PGJ_2 binds covalently to tubulin and that this binding is probably the cause of microtubule depolymerization in 15d-PGJ_2-treated MCF-7 cells. Our results show that 15d-PGJ_2 binds covalently to at least, four cysteine residues into the α- and β-tubulin moieties, as detected by mass spectrometry. 15d-PGJ_2 is characterized by the presence of a cyclopentenone ring containing an electrophilic carbon (C9), and an electrophilic unsaturated carbonyl group (C13) next to the cyclopentenone ring. These two chemically reactive centers can react covalently by means of Michael's addition reaction with nucleophiles, such as the cysteinyl thiol groups in proteins, to form a covalent adduct which is thought to be irreversible under physiological conditions. Some examples of 15d-PGJ_2 Michael's addition to cysteine residues include PPARγ (reactive carbon at position 13) and NF-κB (reactive carbon at position 9) proteins [48].

Tubulin is a heterodimeric protein containing 20 cysteine residues, of which twelve are in the α subunit and eight in the β subunit. Five of these cysteines have been characterized as highly reactive [49]. We have shown here that, at least four of them react with 15d-PGJ_2. Cysteine 305 from β-tubulin is located on the surface of the microtubule near the pore, and probably does not have any effect on microtubule stability. In contrast, cysteines 241 and 356 are located at the inner face, between the GTP and the taxol binding sites, and the binding of 15d-PGJ_2 to these residues could alter the normal curvature of the heterodimer, inducing the microtubule depolymerization. In addition, cysteine 316 from α-tubulin is located in the interphase between an α-subunit and a β-subunit, and, consequently, it is very likely that 15d-PGJ_2-binding to this residue could also interfere in the microtubule assembly. Thus,

ACCEPTED MANUSCRIPT

covalent binding of 15d-PGJ_2 to cysteine residues in microtubules is probably the cause of the observed microtubules depolymerization.

In summary, our data add a new anti-tumoral role for 15d-PGJ_2 based on the ability to directly binding to cysteine residues in α- and β-tubulin independently of PPARγ. As a consequence, 15d-PGJ_2 disrupts the MT structure in the cytoplasm of interphase cells and the spindle apparatus of mitotic cells leading to a mitotic arrest at the metaphase/anaphase transition, an accumulation of cells in G_2/M phase, and ultimately breast cancer cell death.

Accepted Manuscript

ACCEPTED MANUSCRIPT

ACKNOWLEDGMENTS

This work was supported by the Ministerio de Educacion y Ciencia grants SAF2004-06263-CO2-01 and SAF2007-62811 (to A.P.-C) and SAF2004-06263-CO2-02 (to A.S.), and the Fondo de Investigaciones Sanitarias grant PIO40682 (to A.P.-C). CIBERNED is founded by the Instituto de Salud Carlos III. The authors thank Dr. Alberto Alvarez-Barrientos for his help in the flow cytometry analysis. C.C was a postdoctoral fellow from the Ministerio de Educación y Ciencia of Spain. J.D. is a fellow of the Fondo de Investigaciones Sanitarias de la Seguridad Social.

ABBREVIATIONS

MS, mass spectrometry; MT, microtubules; PPARγ, peroxisome proliferators-activated receptor γ; RSG, rosiglitazone; 15d-PGJ_2, 15-deoxi-$\Delta^{12,14}$-prostaglandin J_2

Accepted Manuscript

ACCEPTED MANUSCRIPT

REFERENCES

[1] Gilroy DW, Colville-Nash PR, Willis D, Chivers J, Paul-Clark MJ, Willoughby DA. Inducible cyclooxygenase may have anti-inflammatory properties. Nature medicine 1999;5:698-701.

[2] Negishi M, Katoh H. Cyclopentenone prostaglandin receptors. Prostaglandins Other Lipid Mediat 2002;68-69:611-7.

[3] Straus DS, Glass CK. Cyclopentenone prostaglandins: new insights on biological activities and cellular targets. Med Res Rev 2001;21:185-210.

[4] Butler R, Mitchell SH, Tindall DJ, Young CY. Nonapoptotic cell death associated with S-phase arrest of prostate cancer cells via the peroxisome proliferator-activated receptor gamma ligand, 15-deoxy-delta12,14-prostaglandin J2. Cell Growth Differ 2000;11:49-61.

[5] Clay CE, Namen AM, Atsumi G, Willingham MC, High KP, Kute TE, et al. Influence of J series prostaglandins on apoptosis and tumorigenesis of breast cancer cells. Carcinogenesis 1999;20:1905-11.

[6] Nencioni A, Lauber K, Grunebach F, Van Parijs L, Denzlinger C, Wesselborg S, et al. Cyclopentenone prostaglandins induce lymphocyte apoptosis by activating the mitochondrial apoptosis pathway independent of external death receptor signaling. J Immunol 2003;171:5148-56.

[7] Pignatelli M, Cortes-Canteli M, Lai C, Santos A, Perez-Castillo A. The peroxisome proliferator-activated receptor gamma is an inhibitor of ErbBs activity in human breast cancer cells. J Cell Sci 2001;114:4117-26.

[8] Pignatelli M, Sanchez-Rodriguez J, Santos A, Perez-Castillo A. 15-Deoxy-{Delta}-12,14-prostaglandin J2 induces programmed cell death of breast cancer cells by a pleiotropic mechanism. Carcinogenesis 2005;26:81-92.

[9] Shimada T, Kojima K, Yoshiura K, Hiraishi H, Terano A. Characteristics of the peroxisome proliferator activated receptor gamma (PPARgamma) ligand induced apoptosis in colon cancer cells. Gut 2002;50:658-64.

ACCEPTED MANUSCRIPT

[10] Tsubouchi Y, Sano H, Kawahito Y, Mukai S, Yamada R, Kohno M, et al. Inhibition of human lung cancer cell growth by the peroxisome proliferator-activated receptor-gamma agonists through induction of apoptosis. Biochemical and biophysical research communications 2000;270:400-5.

[11] Zander T, Kraus JA, Grommes C, Schlegel U, Feinstein D, Klockgether T, et al. Induction of apoptosis in human and rat glioma by agonists of the nuclear receptor PPARgamma. Journal of neurochemistry 2002;81:1052-60.

[12] Kliewer SA, Lenhard JM, Willson TM, Patel I, Morris DC, Lehmann JM. A prostaglandin J2 metabolite binds peroxisome proliferator-activated receptor gamma and promotes adipocyte differentiation. Cell 1995;83:813-9.

[13] Boyault S, Simonin MA, Bianchi A, Compe E, Liagre B, Mainard D, et al. 15-Deoxy-delta12,14-PGJ2, but not troglitazone, modulates IL-1beta effects in human chondrocytes by inhibiting NF-kappaB and AP-1 activation pathways. FEBS letters 2001;501:24-30.

[14] Ward C, Dransfield I, Murray J, Farrow SN, Haslett C, Rossi AG. Prostaglandin D2 and its metabolites induce caspase-dependent granulocyte apoptosis that is mediated via inhibition of I kappa B alpha degradation using a peroxisome proliferator-activated receptor-gamma-independent mechanism. J Immunol 2002;168:6232-43.

[15] Gilroy DW, Lawrence T, Perretti M, Rossi AG. Inflammatory resolution: new opportunities for drug discovery. Nat Rev Drug Discov 2004;3:401-16.

[16] Castrillo A, Diaz-Guerra MJ, Hortelano S, Martin-Sanz P, Bosca L. Inhibition of IkappaB kinase and IkappaB phosphorylation by 15-deoxy-Delta(12,14)-prostaglandin J(2) in activated murine macrophages. Mol Cell Biol 2000;20:1692-8.

[17] Clay CE, Monjazeb A, Thorburn J, Chilton FH, High KP. 15-Deoxy-delta12,14-prostaglandin J2-induced apoptosis does not require PPARgamma in breast cancer cells. J Lipid Res 2002;43:1818-28.

[18] Li L, Tao J, Davaille J, Feral C, Mallat A, Rieusset J, et al. 15-deoxy-Delta 12,14-prostaglandin J2 induces apoptosis of human hepatic myofibroblasts. A pathway involving

Accepted Manuscript

ACCEPTED MANUSCRIPT

oxidative stress independently of peroxisome-proliferator-activated receptors. J Biol Chem 2001;276:38152-8.

[19] Nencioni A, Lauber K, Grunebach F, Brugger W, Denzlinger C, Wesselborg S, et al. Cyclopentenone prostaglandins induce caspase activation and apoptosis in dendritic cells by a PPAR-gamma-independent mechanism: regulation by inflammatory and T cell-derived stimuli. Experimental hematology 2002;30:1020-8.

[20] Martinez B, Perez-Castillo A, Santos A. The mitochondrial respiratory complex I is a target for 15-deoxy-D-12,14-prostaglandin J2 (15d-PGJ2) action. JLipid Res 2005.

[21] Jordan MA, Wilson L. Microtubules as a target for anticancer drugs. Nature reviews 2004;4:253-65.

[22] Pellegrini F, Budman DR. Review: tubulin function, action of antitubulin drugs, and new drug development. Cancer investigation 2005;23:264-73.

[23] Downing KH. Structural basis for the interaction of tubulin with proteins and drugs that affect microtubule dynamics. Annual review of cell and developmental biology 2000;16:89-111.

[24] Wilson L, Panda D, Jordan MA. Modulation of microtubule dynamics by drugs: a paradigm for the actions of cellular regulators. Cell structure and function 1999;24:329-35.

[25] Minotti AM, Barlow SB, Cabral F. Resistance to antimitotic drugs in Chinese hamster ovary cells correlates with changes in the level of polymerized tubulin. J Biol Chem 1991;266:3987-94.

[26] Bu W, Su LK. Regulation of microtubule assembly by human EB1 family proteins. Oncogene 2001;20:3185-92.

[27] Schneeweiss A, Sinn HP, Ehemann V, Khbeis T, Neben K, Krause U, et al. Centrosomal aberrations in primary invasive breast cancer are associated with nodal status and hormone receptor expression. International journal of cancer 2003;107:346-52.

[28] Buey RM, Calvo E, Barasoain I, Pineda O, Edler MC, Matesanz R, et al. Cyclostreptin binds covalently to microtubule pores and lumenal taxoid binding sites. Nat Chem Biol 2007;3:117-25.

Accepted Manuscript

ACCEPTED MANUSCRIPT

[29] Pignatelli M, Cocca C, Santos A, Perez-Castillo A. Enhancement of BRCA1 gene expression by the peroxisome proliferator-activated receptor gamma in the MCF-7 breast cancer cell line. Oncogene 2003;22:5446-50.

[30] Chaffer CL, Thomas DM, Thompson EW, Williams ED. PPARgamma-independent induction of growth arrest and apoptosis in prostate and bladder carcinoma. BMC Cancer 2006;6:53.

[31] Kim EH, Na HK, Kim DH, Park SA, Kim HN, Song NY, et al. 15-Deoxy-Delta12,14-prostaglandin J2 induces COX-2 expression through Akt-driven AP-1 activation in human breast cancer cells: a potential role of ROS. Carcinogenesis 2008;29:688-95.

[32] Badano JL, Teslovich TM, Katsanis N. The centrosome in human genetic disease. Nature reviews 2005;6:194-205.

[33] Sankaran S, Parvin JD. Centrosome function in normal and tumor cells. J Cell Biochem 2006;99:1240-50.

[34] Srsen V, Merdes A. The centrosome and cell proliferation. Cell Div 2006;1:26.

[35] Pihan GA, Purohit A, Wallace J, Knecht H, Woda B, Quesenberry P, et al. Centrosome defects and genetic instability in malignant tumors. Cancer Res 1998;58:3974-85.

[36] Schneeweiss A, Sinn HP, Ehemann V, Khbeis T, Neben K, Krause U, et al. Centrosomal aberrations in primary invasive breast cancer are associated with nodal status and hormone receptor expression. International journal of cancer 2003;107:346-52.

[37] Pihan GA, Purohit A, Wallace J, Malhotra R, Liotta L, Doxsey SJ. Centrosome defects can account for cellular and genetic changes that characterize prostate cancer progression. Cancer Res 2001;61:2212-9.

[38] Schneider Y, Chabert P, Stutzmann J, Coelho D, Fougerousse A, Gosse F, et al. Resveratrol analog (Z)-3,5,4'-trimethoxystilbene is a potent anti-mitotic drug inhibiting tubulin polymerization. International journal of cancer 2003;107:189-96.

[39] Jordan MA. Mechanism of action of antitumor drugs that interact with microtubules and tubulin. Current medicinal chemistry 2002;2:1-17.

Accepted Manuscript

ACCEPTED MANUSCRIPT

[40] Wilson L, Jordan MA. Microtubule dynamics: taking aim at a moving target. Chem Biol 1995;2:569-73.

[41] Lin HL, Chang YF, Liu TY, Wu CW, Chi CW. Submicromolar paclitaxel induces apoptosis in human gastric cancer cells at early G1 phase. Anticancer Res 1998;18:3443-9.

[42] Jordan MA, Wendell K, Gardiner S, Derry WB, Copp H, Wilson L. Mitotic block induced in HeLa cells by low concentrations of paclitaxel (Taxol) results in abnormal mitotic exit and apoptotic cell death. Cancer Res 1996;56:816-25.

[43] Woods CM, Zhu J, McQueney PA, Bollag D, Lazarides E. Taxol-induced mitotic block triggers rapid onset of a p53-independent apoptotic pathway. Mol Med 1995;1:506-26.

[44] Huang Y, Johnson KR, Norris JS, Fan W. Nuclear factor-kappaB/IkappaB signaling pathway may contribute to the mediation of paclitaxel-induced apoptosis in solid tumor cells. Cancer Res 2000;60:4426-32.

[45] Miller MC, 3rd, Johnson KR, Willingham MC, Fan W. Apoptotic cell death induced by baccatin III, a precursor of paclitaxel, may occur without G(2)/M arrest. Cancer Chemother Pharmacol 1999;44:444-52.

[46] Nabha SM, Mohammad RM, Dandashi MH, Coupaye-Gerard B, Aboukameel A, Pettit GR, et al. Combretastatin-A4 prodrug induces mitotic catastrophe in chronic lymphocytic leukemia cell line independent of caspase activation and poly(ADP-ribose) polymerase cleavage. Clin Cancer Res 2002;8:2735-41.

[47] Kanthou C, Greco O, Stratford A, Cook I, Knight R, Benzakour O, et al. The tubulin-binding agent combretastatin A-4-phosphate arrests endothelial cells in mitosis and induces mitotic cell death. Am J Pathol 2004;165:1401-11.

[48] Kim EH, Surh YJ. 15-deoxy-Delta12,14-prostaglandin J2 as a potential endogenous regulator of redox-sensitive transcription factors. Biochem Pharmacol 2006;72:1516-28.

[49] Britto PJ, Knipling L, Wolff J. The local electrostatic environment determines cysteine reactivity of tubulin. J Biol Chem 2002;277:29018-27.

Accepted Manuscript

ACCEPTED MANUSCRIPT

FIGURE LEGENDS

Figure 1. Effect of 15d-PGJ_2 and rosiglitazone on cell cycle distribution of exponentially dividing MCF-7 cells. The numbers indicate the percentage ± SD of cells in each phase of the cell cycle. Cells were exposed to 10 μM 15d-PGJ_2, 30 μM rosiglitazone (RSG) or 1 μM nocodazole for 24 h and DNA flow cytometry was performed on cells. Data are representative of three independent experiments. *, $P < 0.05$; *** $P < 0.001$.

Figure 2. Disruption of microtubules in 15d-PGJ_2-treated MCF-7 cells. (A) Cells were treated for 12 h with 1 μM nocodazole, 10 μM 15d-PGJ_2 or 30 μM rosiglitazone (RSG), fixed and stained with anti-α-tubulin and anti-pericentrin. DNA was stained with DAPI. Scale bar, 10 μm. (B) Polymerized tubulin (P) was differentially extracted from soluble (S) tubulin in control, rosiglitazone (RSG)- and 15d-PGJ_2-treated MCF-7 cell lysates prepared in a MT-stabilizing buffer. Soluble and polymerized tubulin fractions were then analyzed by blotting for α-tubulin. (C) Tubulin bands were quantified by densitometric analysis and expressed as a percentage of total tubulin levels. *, $P < 0.05$.

Figure 3. Treatment of MCF-7 cells with 15d-PGJ_2 perturbs mitotic progression. Control (A) and cells treated for 24 h with 15d-PGJ_2 (B) were fixed and stained with anti-α-tubulin and anti-pericentrin. DNA was stained with DAPI. Shown are representative confocal images of MCF-7 cells mitotic progression. Scale bar, 10 μm. (C) Frequency of mitotic stages in control and 15d-PGJ_2-treated MCF-7 cells was quantified and expressed as a percentage of total cells. ***, $P < 0.001$.

Accepted Manuscript

ACCEPTED MANUSCRIPT

Figure 4. Analysis of mitosis in live MCF-7 cells. Representative images from time-lapse analysis of live cells showing the different phases of mitosis are shown. Time zero, shown in minutes, is the time point at which the nuclear envelope is breakdown and chromatin condensation is evident, just at prophase onset. Cultures were incubated with 10 μM 15d-PGJ_2 or 30 μM rosiglitazone (RSG) and areas were subsequently followed by time-lapse microscopy. Cells treated with 15d-PGJ_2 remained in metaphase for more than 8 h afterward they die. In contrast, non-treated- and rosiglitazone-treated cells escaped mitosis after ~ 1 h. Scale bars, 50 (lower magnification) and 10 (higher magnification) μm. Time-lapse movies for the sequential images shown in this Fig. can be found online.

Figure 5. Effect of 15d-PGJ_2 on tubulin polymerization in vitro. Purified bovine brain tubulin was incubated in the presence of buffer (blank), 1 μM nocodazole, 10 μM 15d-PGJ_2, or 200 μM paclitaxel at 37ºC, and absorbance readings were recorded at 340 nm each 30 s for 1 h. Data are representative of two independent experiments performed in triplicate.

Figure 6. Binding of biotinilated 15d-PGJ_2 to α- and β-tubulin *in vivo*. (A) MCF-7 cells were incubated or not with biotinilated 15d-PGJ_2 for 2 h and cell lysates were subjected to pull-down assays with Neutravidin-gel beads. The presence of α- and β-tubulin was assessed by Western blot analysis with specific antibodies. (B) MCF-7 cells were treated as in A and cellular accumulation of biotinylated 15d-PGJ_2 was evaluated by confocal microscopy. Tubulin was detected with a specific mouse monoclonal antibody and 15d-PGJ_2 with an anti-biotin antibody. Scale bar, 10 μm. (C) Same staining as in B, showing colocalisation of biotynilated 15d-PG_2 in mitotic cells. Scale bar, 20 μm.

Accepted Manuscript

ACCEPTED MANUSCRIPT

Figure 7**.** MS analyses of 15d-PGJ$_2$ binding to microtubules. Total ion chromatogram (TIC) of the precursor ion scanning of fragment at m/z 299.4 from control (A, upper panel) or 15d-PGJ$_2$-treated (A, lower panel) microtubules samples, digested with trypsin. Arrows labeled as 1-4 indicate retention times corresponding to different peptide mass composition between control and 15d-PGJ$_2$-treated microtubules samples. These differences are detailed in (B) with labels 1-4 indicating the 15d-PGJ$_2$-modified sequences. C means control-, and PG means 15d-PGJ$_2$-treated microtubules samples. Differential masses absent in the control mass spectrum are labeled as an (*). Peaks 5 and 6 correspond to differential chromatographic peaks. Peak 5 contains the peptide with sequence 309-HGKYMACC^{PG}LLYR-320 (one missed cleavage at K311). Peak 6 corresponds to the 15d-PGJ$_2$ dimer.

Figure 8**.** MRM experiments with control and 15d-PGJ$_2$-treated microtubules samples. MRM experiments from tryptic, 15d-PGJ$_2$-modified peptides 1-4. The inset shows the MRM results for the corresponding control microtubules sample.

Accepted Manuscript

Figure

Figure 1

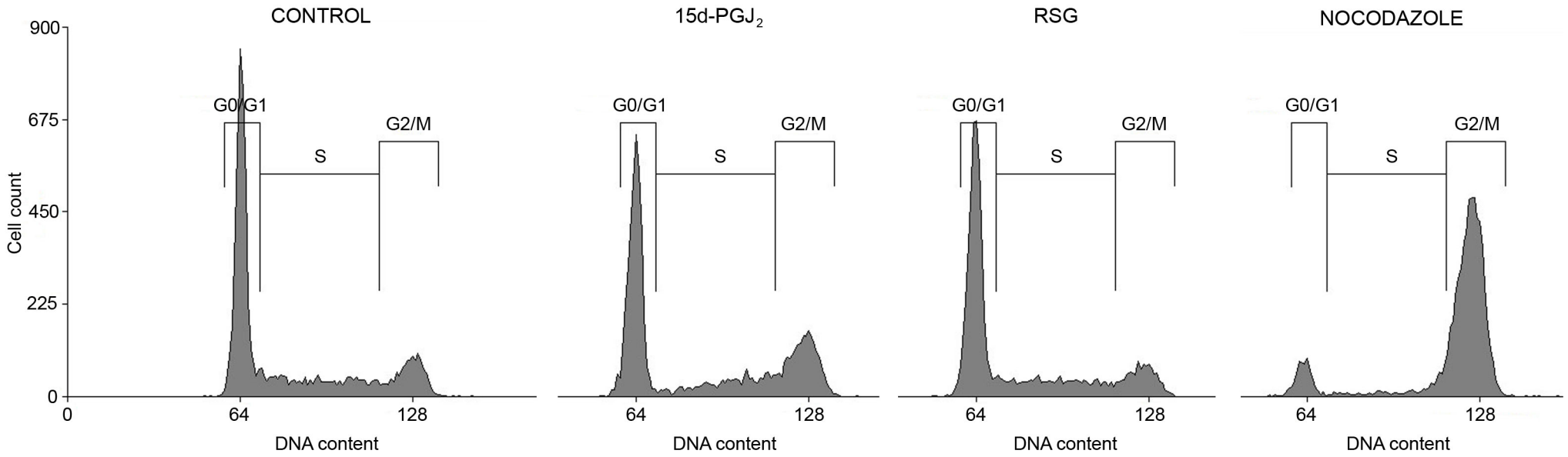

	G0/G1	S	G2/M (%)
Control	55.67 ±2.52	25.50 ± 1.50	17.10 ± 1.15
15d-PGJ_2	44.67 ± 5.69 *	15.00 ± 4.36 *	38.33 ± 2.52 ***
RSG	57.44 ± 1.39	21.67 ± 3.51	19.28 ± 3.09
Nocodazole	6.23 ± 3.61 ***	12.26 ± 1.65 *	79.44 ± 1.81 ***

Figure 2

A

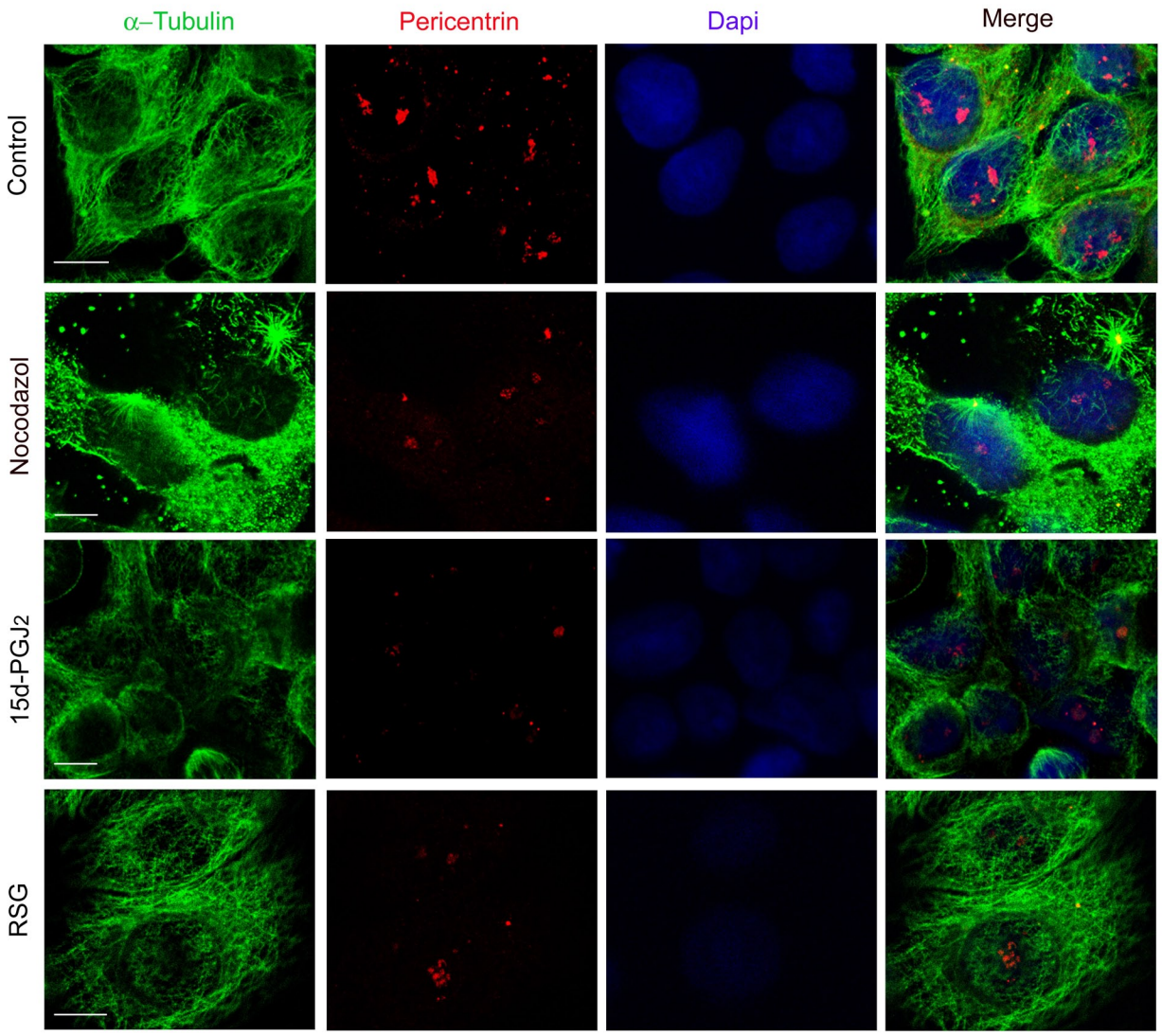
α–Tubulin
Pericentrin
Dapi
Merge
Control
Nocodazol
15d-PGJ2
RSG

B

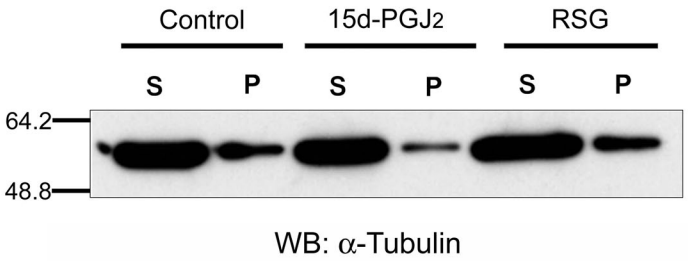
Control
15d-PGJ2
RSG
S
P
S
P
S
P
64.2
48.8
WB: α-Tubulin

C

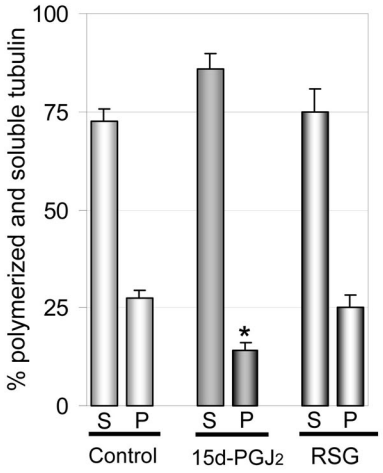
% polymerized and soluble tubulin
100
75
50
25
0
*
S
P
S
P
S
P
Control
15d-PGJ2
RSG

Figure 3

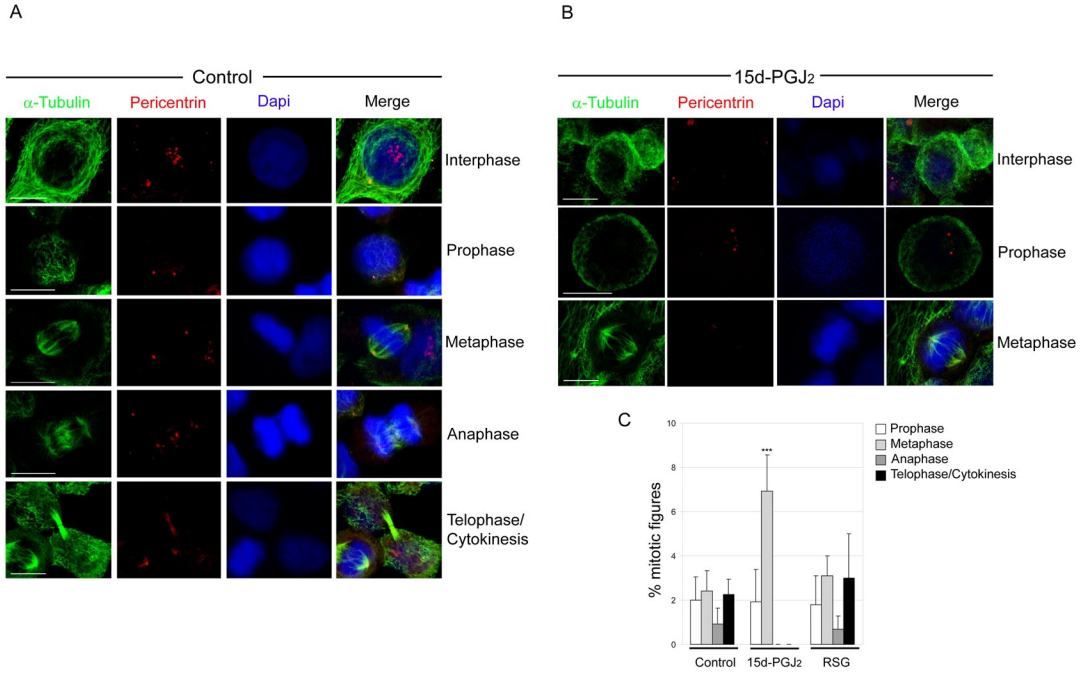
A
Control
α-Tubulin
Pericentrin
Dapi
Merge
Interphase
Prophase
Metaphase
Anaphase
Telophase/
Cytokinesis
B
15d-PGJ2
α-Tubulin
Pericentrin
Dapi
Merge
Interphase
Prophase
Metaphase
C
% mitotic figures
10
8
6
4
2
0
***
Prophase
Metaphase
Anaphase
Telophase/Cytokinesis
Control
15d-PGJ2
RSG

Figure 4

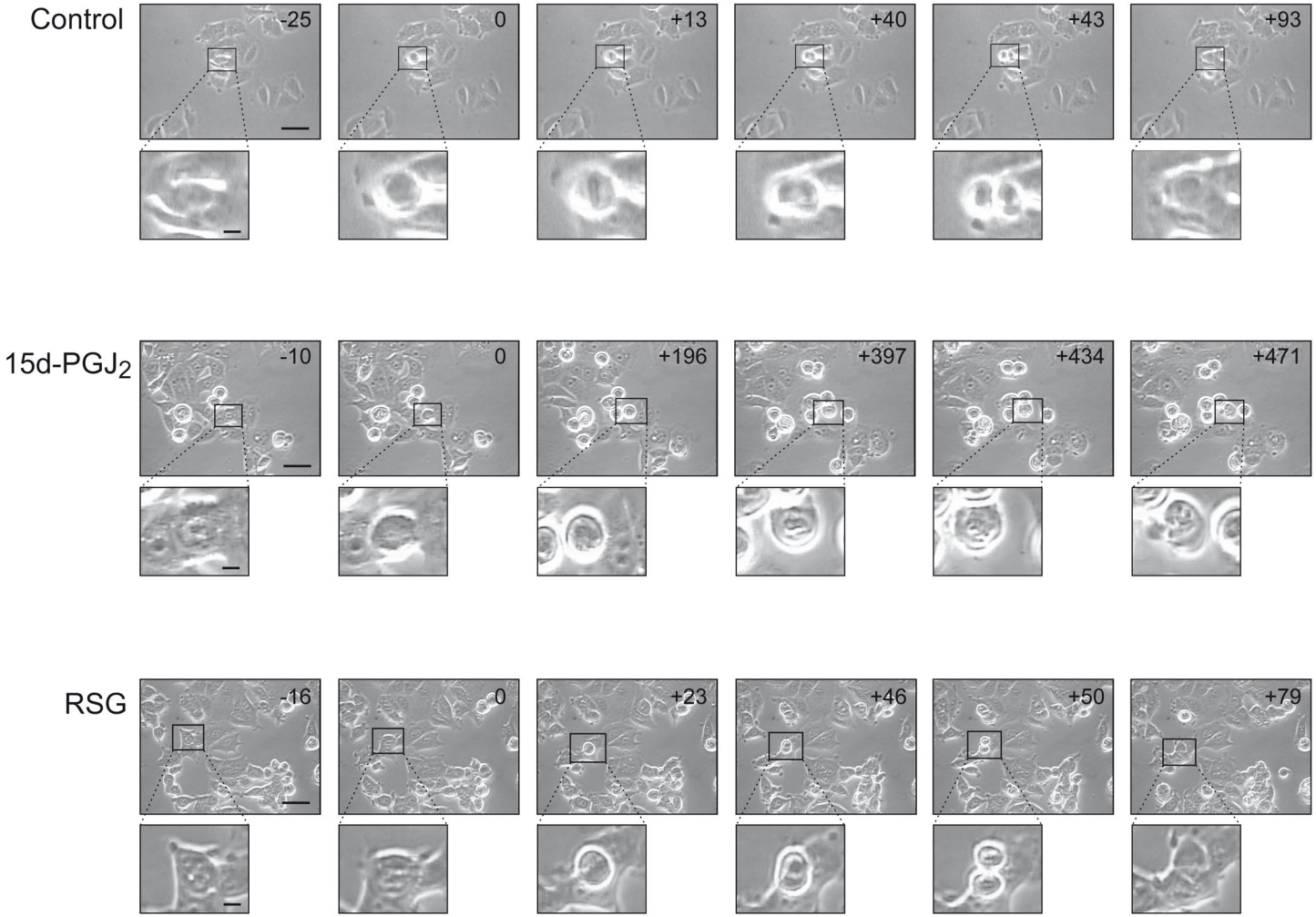
Control
-25
0
+13
+40
+43
+93
15d-PGJ2
-10
0
+196
+397
+434
+471
RSG
-16
0
+23
+46
+50
+79

Figure 5

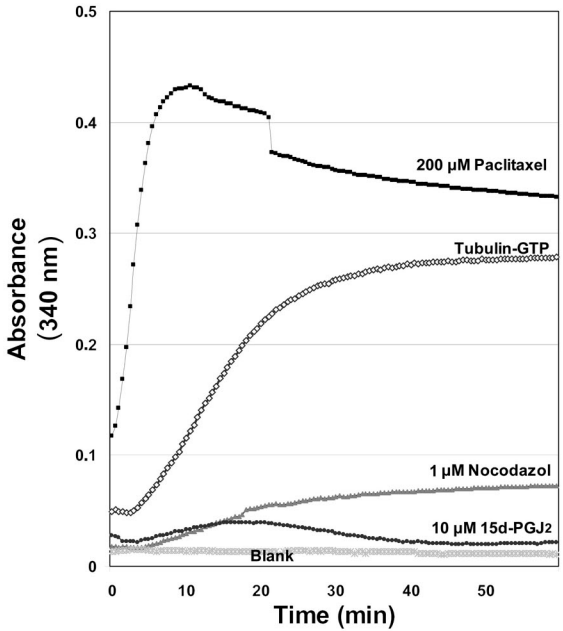
0.5
0.4
0.3
0.2
0.1
0
Absorbance
(340 nm)
200 μM Paclitaxel
Tubulin-GTP
1 μM Nocodazol
10 μM 15d-PGJ2
Blank
0
10
20
30
40
50
Time (min)

Figure 6

A

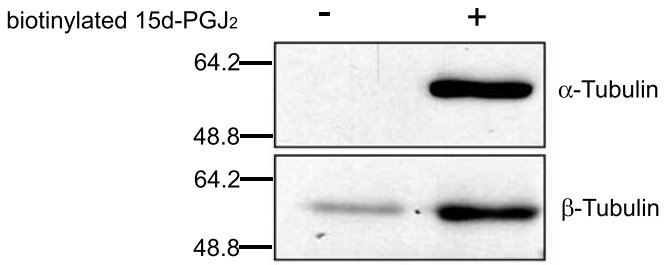

Pull down: Neutravidin

B

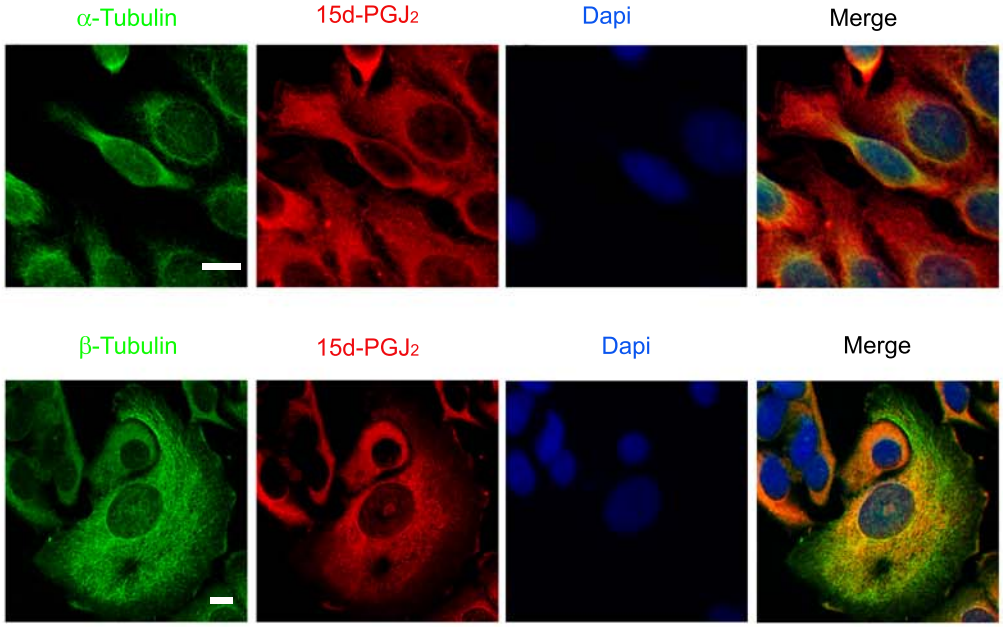

C

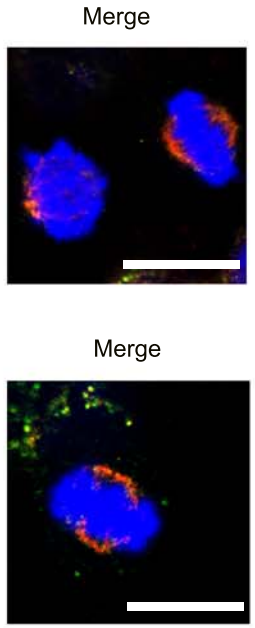

Figure 7

A

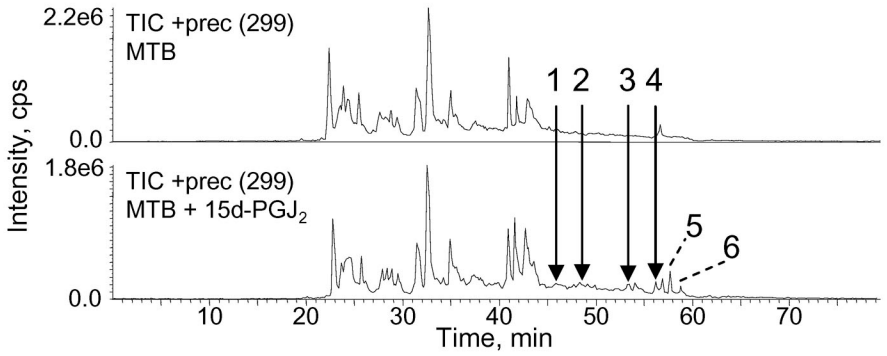
2.2e6
TIC +prec (299)
MTB
0.0
1.8e6
TIC +prec (299)
MTB + 15d-PGJ2
0.0
Intensity, cps
1 2 3 4
5
6
10 20 30 40 50 60 70
Time, min

B

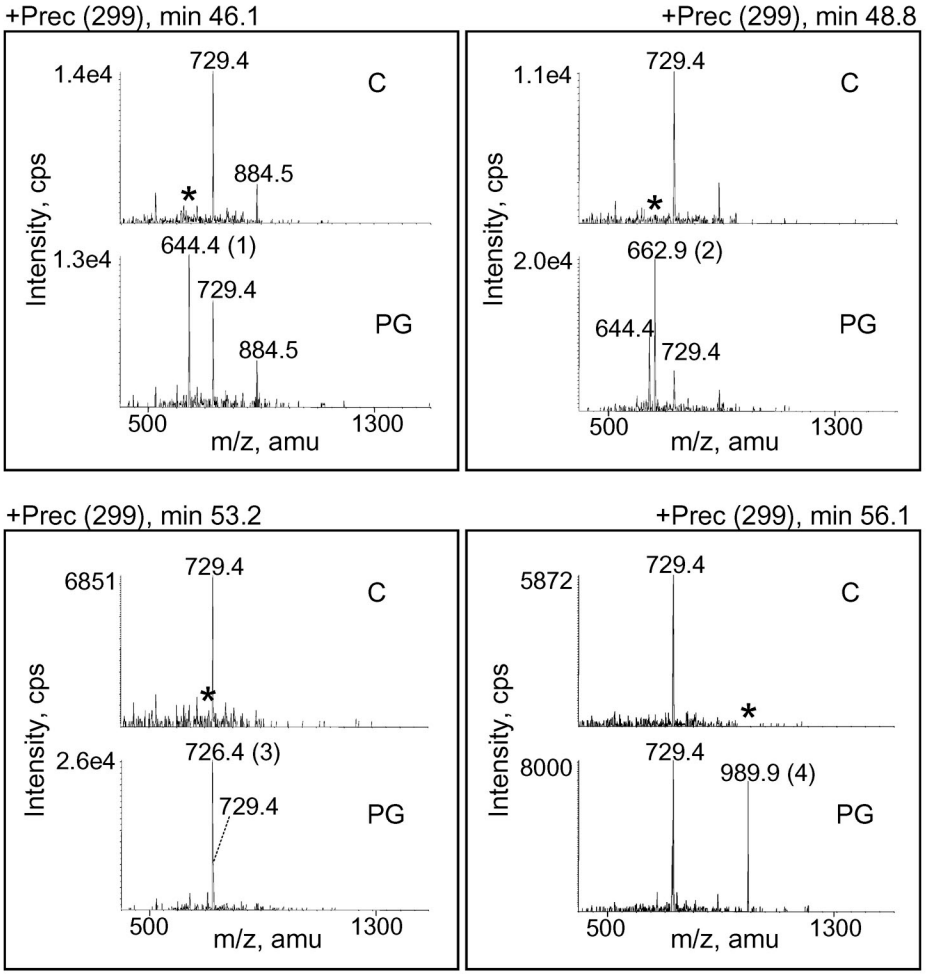
+Prec (299), min 46.1
1.4e4
729.4
C
884.5
*
1.3e4
644.4 (1)
729.4
PG
884.5
500
1300
m/z, amu
Intensity, cps
+Prec (299), min 48.8
1.1e4
729.4
C
*
2.0e4
662.9 (2)
644.4
729.4
PG
500
1300
m/z, amu
Intensity, cps
+Prec (299), min 53.2
6851
729.4
C
*
2.6e4
726.4 (3)
729.4
PG
500
1300
m/z, amu
Intensity, cps
+Prec (299), min 56.1
5872
729.4
C
*
8000
729.4
989.9 (4)
PG
500
1300
m/z, amu
Intensity, cps

Figure 8

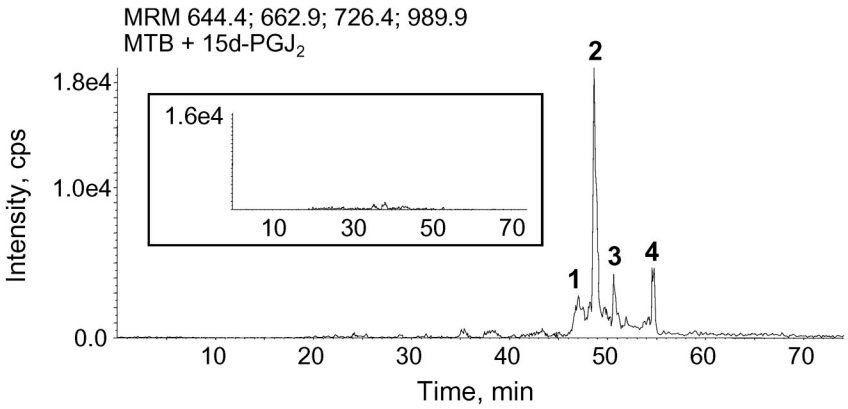
MRM 644.4; 662.9; 726.4; 989.9
MTB + 15d-PGJ2
Intensity, cps
1.8e4
1.0e4
0.0
1.6e4
10
30
50
70
1
2
3
4
10
20
30
40
50
60
70
Time, min

ACCEPTED MANUSCRIPT

Supplemental Figure 1. *Off line* nanospray characterization of 15d-PGJ2 by triple quadrupole MS. An ion at m/z 317.3 Da, corresponding to the monoisotopic, protonated 15d-PGJ_2 molecule, was observed (A). In order to find the main fragments corresponding to single or multiple cleavage sites within the 15d-PGJ_2 molecule, an enhanced product ion experiment was performed. The ion at m/z 317.3 Da was isolated and fragmented (B). The most intense fragment ions were selected as potential markers for later precursor ion scanning experiments in order to find the best marker mass to select precursor ions for filtration of peptides that were tagged with 15d-PGJ_2. The fragment ion at m/z 299.4 Da was the signal of choice for precursor ion filtering experiments (C). The efficiency of precursor ion scanning experiments was lower when using other fragment ions present in the MS/MS spectrum from the 15d-PGJ_2 molecule (black arrows) (C).

Supplemental Figure 2. **Characterization of 15d-PGJ_2 binding site by triple quadrupole MS.** The figure displays the main fragmentation series (carboxy, y, and amino, b, series) for the doubly-charged parent ions from peak 1-3 (A-C, respectively), and for the triply-charged parent ion from peak 4 (D). On each panel the corresponding peptide sequence is shown, as well as fragments containing the 15d-PGJ_2 (superscripted PG). Numbers in boxes (including the filtering mass at m/z 299.4 Da for the precursor ion scanning experiments) indicate masses resulting from fragmentation of the 15d-PGJ_2 molecule. Water loss of some fragments are marked with an (*), and some secondary fragmentation series peptides (a series) are also indicated.

Supplemental Video 1. **Mitosis progression in control MCF-7 cells**. Time-lapse sequence taken from control MCF-7 cells progressing through mitosis. Images were collected every minute, and the movie runs at 7 frames per second. Bar, 50 μm. Video corresponds to the cell shown in Figure 4 (two upper panels).

Supplemental Video 2. **Mitosis progression in 15d-PGJ_2-treated MCF-7 cells.** Time-lapse sequence taken from MCF-7 cells progressing through mitosis in the presence of 15d-PGJ_2. Images were collected every minute, and the movie runs at 7 frames per second. Bar, 50 μm. Video corresponds to the cell shown in Figure 4 (two middle panels).

Accepted Manuscript

ACCEPTED MANUSCRIPT

Supplemental Video 3. **Mitosis progression in rosiglitazone-treated MCF-7 cells** Time-lapse sequence taken from MCF-7 cells progressing through mitosis in the presence of rosiglitazone. Images were collected every minute, and the movie runs at 7 frames per second. Bar, 50 μm. Video corresponds to the cell shown in Figure 4 (two lower panels).

Accepted Manuscript

supplementary figures

Supplementary Figure 1

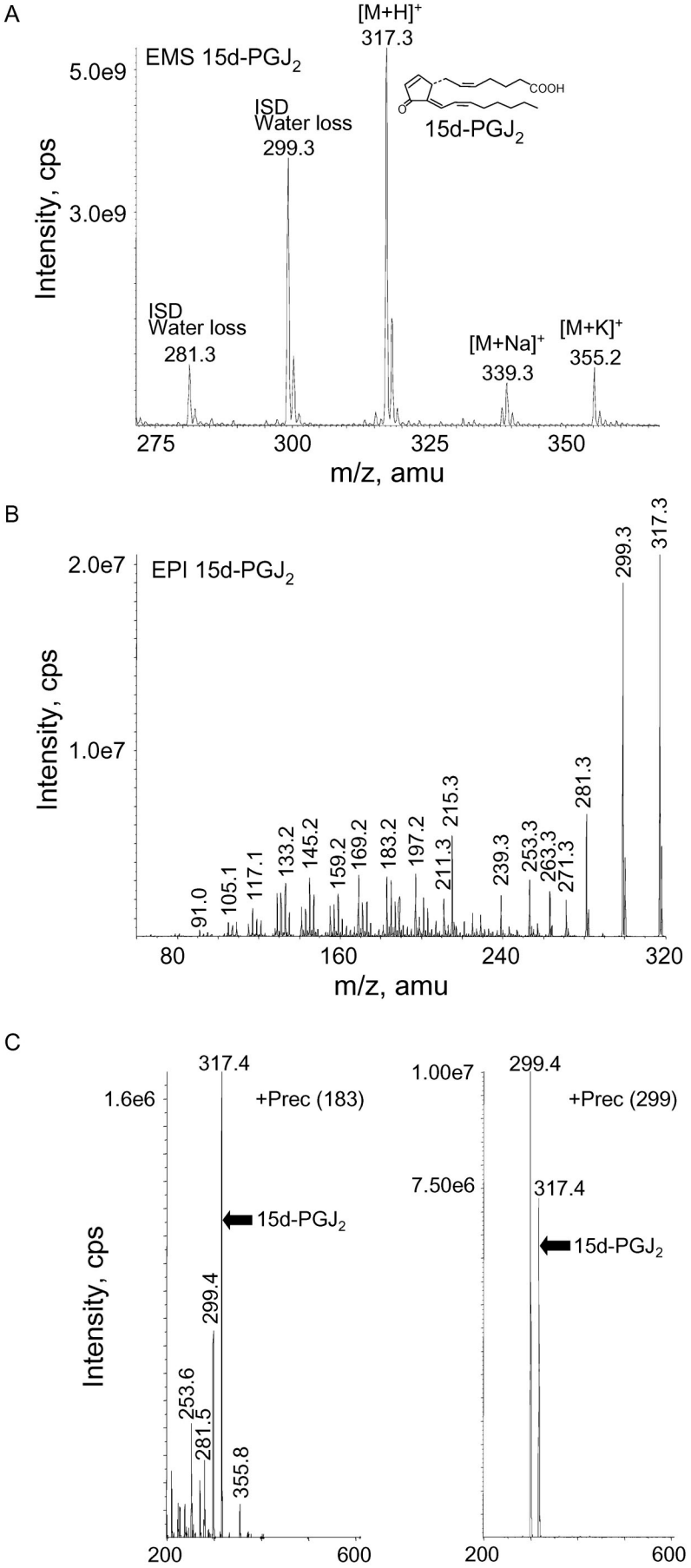

Supplementary Figure 2

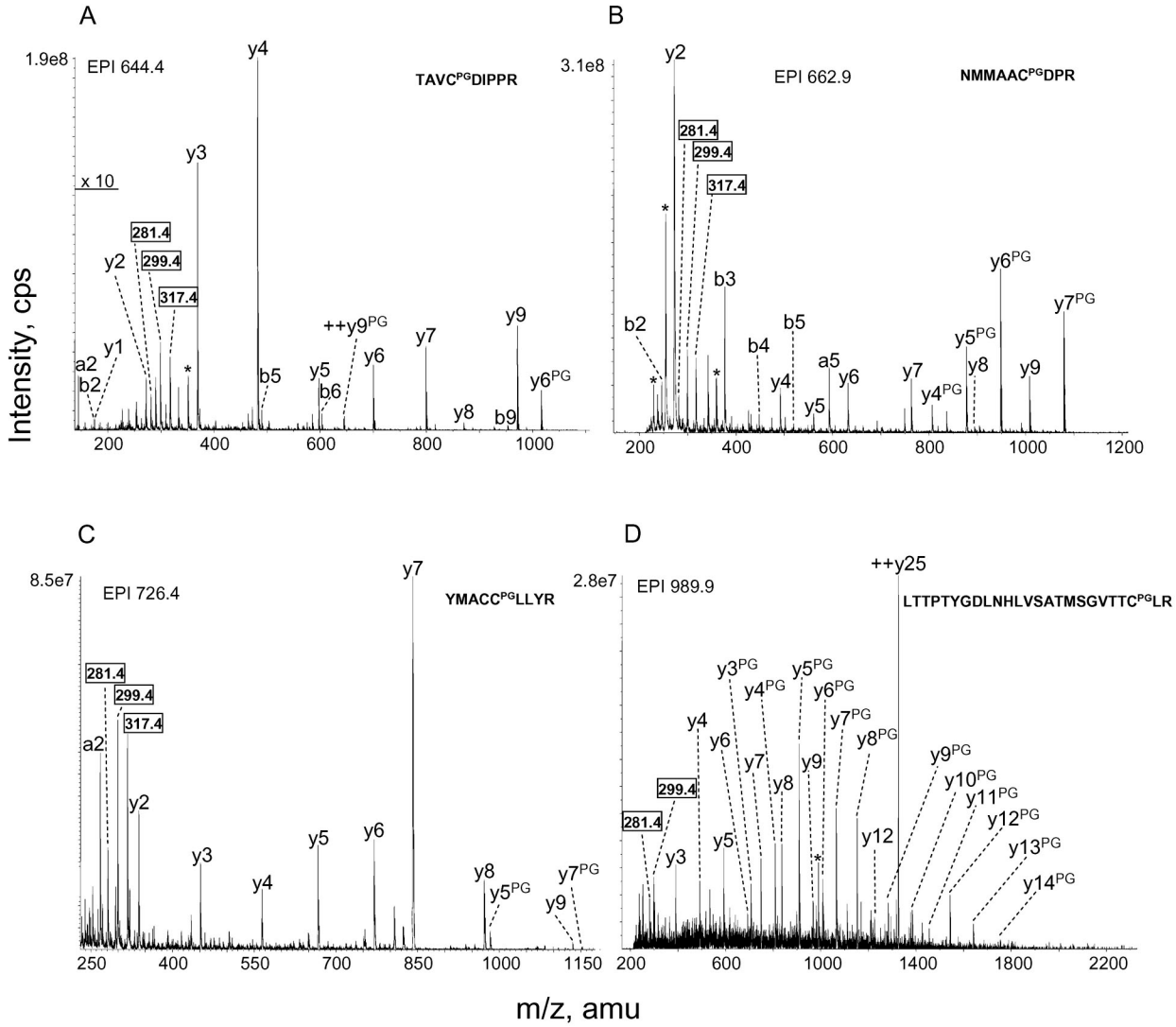
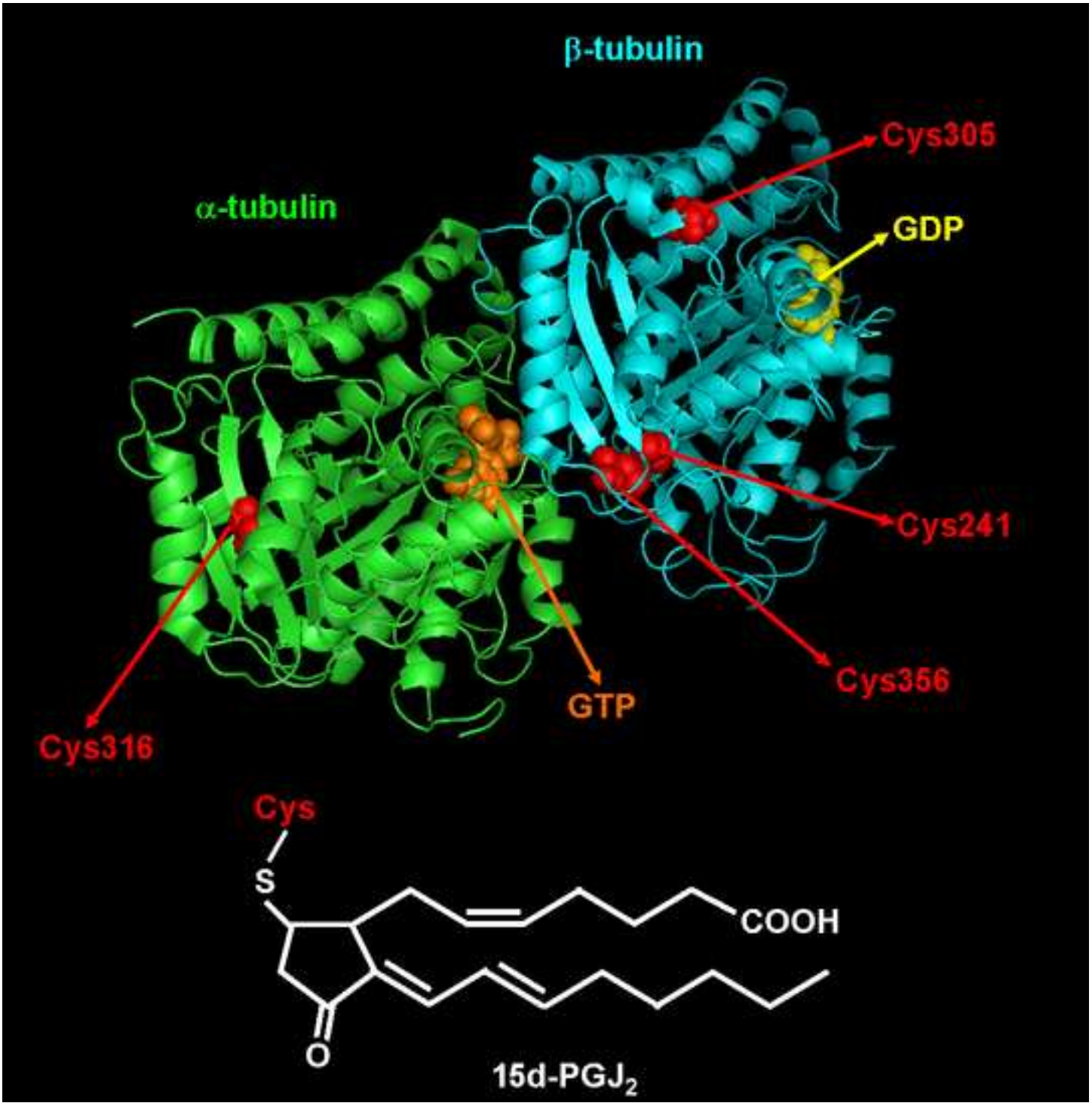
ACCEPTED MANUSCRIPT